

# Non-monotonic diffusion rates in atom-optics Lévy kicked rotor

Sanku Paul,<sup>1</sup> Sumit Sarkar,<sup>2</sup> Chetan Vishwakarma,<sup>2</sup> Jay Mangaonkar,<sup>2</sup> M. S. Santhanam,<sup>2</sup> and Umakant Rapol<sup>2</sup>

<sup>1</sup>*Max-Planck-Institut für Physik komplexer Systeme,  
Nöthnitzer Straße 38, 01187 Dresden, Germany.*

<sup>2</sup>*Indian Institute of Science Education and Research, Homi Bhabha Road, Pune 411 021, India.*

(Dated: January 17, 2022)

The dynamics of chaotic Hamiltonian systems such as the kicked rotor continues to guide our understanding of transport and localization processes. The localized states of the quantum kicked rotor decay due to decoherence effects if subjected to stationary noise. The associated quantum diffusion increases monotonically as a function of a parameter characterising the noise distribution. In this work, for the Lévy kicked atom-optics rotor, it is experimentally shown that by tuning a parameter characterizing the Lévy distribution, quantum diffusion displays non-monotonic behaviour. The parameters for optimal diffusion rates are analytically obtained and they reveal a good agreement with the cold atom experiments and numerics. The non-monotonicity is shown to be a quantum effect that vanishes in the classical limit.

Chaotic Hamiltonian systems continue to open up novel scenarios for momentum and energy transport in both the classical and quantum regimes. The kicked rotor system, a particle periodically kicked by an external sinusoidal field, is a paradigm for Hamiltonian chaos. This sets standard benchmark for momentum transport, namely that, in the regime of sufficiently strong kicking strengths, the onset of quantum interference effects strongly attenuates the classical diffusive transport [1, 2]. This is the dynamical localization scenario in which the system settles to a quasi-steady state and does not absorb energy anymore. In contrast to this, novel transport scenarios have been exemplified by several variants of kicked rotor. These include atom-optics based experimental realizations and theoretical studies of directed transport in parity broken [3], PT symmetric [4] and dissipative [5] kicked rotors. Anomalous transport has been observed in Lévy kicked [6], relativistic [7, 8] and a non-smooth version [9] of kicked rotor, while suppression of quantum diffusive transport was observed in higher dimensional [10], non-ideal [11], coupled [12, 13] and relativistic [14] kicked rotors. As the quantum kicked rotor is related to the Anderson model [15, 16] for charge transport in a crystalline lattice, all these results have applications for a larger class of disordered conductors and time-dependent problems in condensed matter physics.

Kicked rotor is suitable for studying decoherence or the quantum to classical transition of its localized states, especially since the classical and quantum signatures of transport are markedly distinct. In the classical domain, the temporal evolution of mean energy is  $\langle E \rangle = Dt$  where the diffusion coefficient  $D \approx K^2/2$  and  $K$  is the kick strength [1]. In the corresponding quantum regime  $\langle E \rangle$  becomes asymptotically time independent, i.e.,  $\langle E \rangle = D(1 - \exp(-t/t_*))$  where  $t_*$  is the Ehrenfest time-scale over which quantum dynamics follows the classical behaviour. Thus, the numerical values of the kick strength  $K \gg 1$  and kick period  $T$  determine the classical and quantum diffusion rates. In particular, varying  $K$  does not alter the qualitative nature of diffusion except if the accelerator modes are present in the classical phase

space [17, 18]. On the other hand, if the parameters  $K$  and/or  $T$  are subjected to stationary noise, i.e,  $K$  is replaced by  $K + \delta K$ , where  $\delta K$  is drawn from a stationary probability distribution, then both theory and experiments have shown that quantum localization is not sustained [19, 20]. A similar scenario unfolds if  $T$  is subject to an additive noise [21]. In general, the strength of noise serves as a tunable parameter obtained from noise characteristics and increasing it leads to quantum diffusion approaching its classical limit in a monotonic fashion.

In many situations in which conductivity, and not localization, is desired the ability to tune for optimal transport with a fixed kicked strength is useful. From the point of view of atom-optics experimental realizations of kicked rotor, increasing the kick strength requires improved hardware such as additional laser power that may not be always feasible. In this work, we propose a mechanism based on tuning a parameter associated with Lévy-noise characteristics superposed on the kick period  $T$  to obtain optimal momentum transport in an atom-optics kicked rotor system. The optimal diffusion coefficient, as function of a parameter characterising the noise distribution function, is analytically obtained and it is demonstrated through atom-optics based experiment as well.

We consider the dimensionless Hamiltonian of the atom-optics quantum kicked rotor system given by

$$\hat{H} = \hat{p}^2/2 + K \cos \hat{x} \sum_n (1 - g_n) \delta(t - n). \quad (1)$$

In this,  $g_n$  is a stochastic variable that controls if an external field of kick strength  $K$  is applied to the cold atomic cloud at  $n$ -th time instant. Further,  $g_n$  is taken from a discrete Bernoulli distribution such that if  $g_n = 0$ , the particle experience a kick and if  $g_n = 1$  no kick is applied. The waiting time between the occurrences of 0 is drawn from a Lévy waiting time distribution  $w(\tau) \sim \tau^{-1-\alpha}$ , where  $\alpha$  is the Lévy exponent [22, 23]. The regime of  $0 < \alpha < 1$  corresponds to diverging mean waiting time  $\bar{\tau}$  and, as we had demonstrated earlier, this effectively leads to slower decay of decoherence [6]. In this paper, we exploit the dynamics when the kicks are

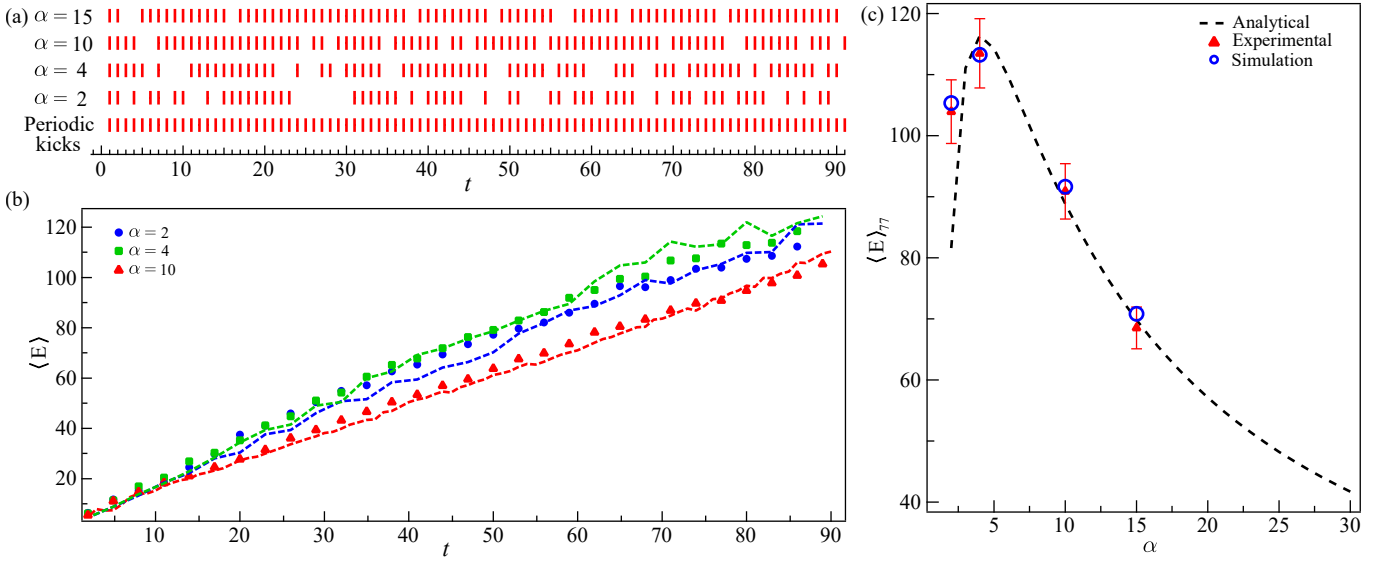


FIG. 1. (a) Schematic diagram representing the sequence of kicks for different  $\alpha$ . (b) Quantum mean energy growth of the system for  $\alpha = 2$ ,  $\alpha = 4$  and  $\alpha = 10$  with  $K = 6.0$ ,  $\hbar_s = 2.0$ . Symbols represent experimental data and solid lines are the numerical results. Experimental data has  $\pm 5\%$  uncertainty (not shown in figure). (c) Represents the behavior of quantum diffusion coefficient by plotting energy after 77 kicks as a function of  $\alpha$  for  $K = 6.0$ ,  $\hbar_s = 2.0$ . Triangular symbols with error bars represent the experimental data, Circular symbols are the numerically calculated values and dashed line is the plot of analytical expression given in Eq. (7) for the break-time  $t^* \approx 5$ , as achieved in our experiment.

imparted at time intervals governed by  $w(\tau)$  with exponent  $\alpha > 1$  and  $\bar{\tau} = \frac{\alpha}{\alpha-1}$  is well defined. In this regime, we demonstrate through both theory and experimentation the existence of an optimal quantum diffusion as a function of  $\alpha$ . This optimality is an unusual property since for other commonly used additive noise sources such as white or Gaussian noise, quantum diffusion is known to be usually monotonic as a function of noise strength [23, 24].

The quantum dynamics of the system in Eq. (1) for  $\alpha > 1$  is studied using the Floquet analysis. The Floquet operator can be written as

$$F(K_n) = e^{-ip^2/2\hbar_s} e^{-iK \cos x/\hbar_s} e^{-iK'_n \cos x/\hbar_s}, \quad (2)$$

$$= F(K) F(K'_n).$$

where  $\hbar_s$  is the scaled Planck's constant,  $K_n = K(1-g_n)$  and  $K'_n = -Kg_n$ . Further,  $F(K)$  represents the Floquet operator of the standard kicked rotor  $F(K) = e^{-ip^2/2\hbar_s} e^{-iK \cos x/\hbar_s}$  for which  $g_n = 0$  for all  $n$ . The noisy rotor corresponds to  $F(K'_n)$ . The starting point of the analysis are the eigenstates  $|r\rangle$  of the Floquet operator  $F(K)$  given by

$$F(K)|r\rangle = e^{-i\eta_r}|r\rangle,$$

where  $\eta_r$  is the quasi-energy of the state  $|r\rangle$ . For  $K \gg 1$  as we have taken,  $\eta_r$  would be the localized states. The factor  $g_n$  induces noise in the kicking sequence whenever  $g_n = 1$  and the kicks are not imparted at those time instants. Thus, under the action of  $F(K'_n)$  system transitions from state  $\eta_r$ . The survival probability amplitude

$A_r(t', t'')$  of the noisy system to remain in the state  $|r\rangle$  in a given time interval  $[t'', t']$  [23] is

$$A_r(t', t'') = \mathcal{N} \left\langle r \left| \mathcal{T} \prod_{n=t''}^{t'-1} F(K_n) \right| r \right\rangle, \quad (3)$$

in which  $\mathcal{T}$  represents time ordering and  $\mathcal{N} = e^{-i\eta_r(t'-t'')}$  is introduced to normalize the survival probability amplitude for the noiseless system.

By using random-phase approximations and performing an average over all the quasi-energy states and also over the random phases of the initial state, the survival probability amplitude to remain in state  $|r\rangle$  for  $\alpha > 1$  takes the form

$$A_r(t', t'') = q \left( K'_n/\hbar_s \right)^{G(t', t'')}. \quad (4)$$

In this,  $G(t', t'')$  represents the number of noisy events in the interval  $[t'', t']$  and

$$q \left( K'_n/\hbar_s \right) = 1 - (K_n'^2/2! \hbar_s^2) \overline{\cos^2(x)} + (K_n'^4/4! \hbar_s^4) \overline{\cos^4(x)} + \dots \quad (5)$$

Thus, it can be inferred that  $|q(K'_n/\hbar_s)| < 1$ , indicating that the survival probability in the state  $|r\rangle$  decays over time and the consequent state transitions result in diffusion. By using the force-force correlator which is related to the decoherence factor [23, 25, 26], the mean energy

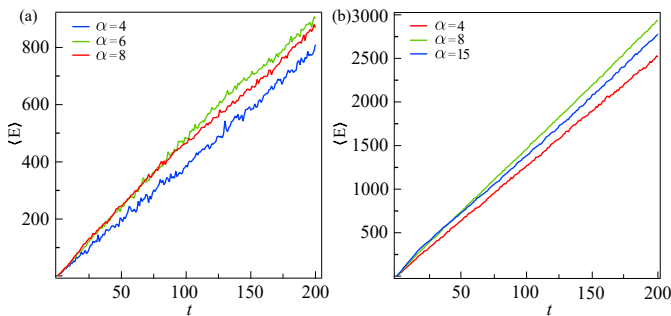


FIG. 2. Numerically calculated mean energy growth of the system for different  $\alpha$  at (a) kick strength  $K = 10$ ,  $\hbar_s = 2$  and (b) kick strength  $K = 15$ ,  $\hbar_s = 2$ .

for  $\alpha > 1$  can be obtained as

$$\begin{aligned} \langle E \rangle_t &\sim \frac{K^2}{2} \left(1 - e^{-\frac{t}{t^*}}\right) - \frac{K^2}{2\alpha} t + \frac{K^2}{2} \frac{t}{1 - \frac{\alpha}{c}} + O(a^t) \\ &\sim I_1 + I_2 + I_3 + O(q^t). \end{aligned} \quad (6)$$

where  $c = (q^2 - 1)t^*$  and  $t^* \sim \frac{K^2}{\hbar_s^2}$  is the break-time of the standard kicked rotor. To physically understand this expression, we analyse each of these terms. The first term ( $I_1 = \frac{K^2}{2} (1 - e^{-\frac{t}{t^*}})$ ) represents the energy growth of the standard kicked rotor,  $I_2 = \left(\frac{K^2}{2\alpha} t\right)$  corresponds to the missing of kicks and the energy growth is represented by  $I_3 + O(q^t) = \left(\frac{K^2}{2} \frac{t}{1 - \frac{\alpha}{c}} + O(a^t)\right)$  results from decoherence due to the introduction of noise.

After long times,  $t \gg t^*$ , Eq. (6) reduces to  $\langle E \rangle \sim Dt$ , in which the diffusion coefficient  $D$  is given by

$$D \sim \frac{K^2}{2} \left(-\frac{1}{\alpha} + \frac{1}{1 - \frac{\alpha}{c}}\right). \quad (7)$$

This reveals a nonlinear dependence of the diffusion coefficient  $D$  on both the kick strength  $K$  and Lévy exponent  $\alpha$ . The mean energy of the system grows linearly in time indicating a dominance of diffusion. In contrast, the diffusion coefficient  $D$  has a quadratic dependence on kick strength but significantly the dependence on  $\alpha$  is not monotonic. The expressions in Eqs. 6-7 form the central analytical results of this paper. In what follows, we describe an atom-optics based experiment to verify these results.

The experimental sequence is similar to that given in Ref. [6]. We prepare a laser-cooled cloud of  $^{87}\text{Rb}$  atoms in magneto-optical trap (MOT). This is followed by further forced evaporative cooling in a crossed optical dipole trap ( $\lambda = 1064\text{nm}$ ). The cold atomic ensemble has  $\sim 2 \times 10^5$  atoms at temperature  $\sim 3 \mu\text{K}$  and follows Maxwell-Boltzmann distribution in momentum space. This atomic ensemble serves as the initial Gaussian wavepacket for simulating the quantum kicked rotor. The process of kicking is implemented using a

pulsating 1-D optical lattice. The lattice laser beam is  $\sim 6.7$  GHz detuned from the  $|F = 1\rangle \rightarrow |F' = 2\rangle$  transition of  $^{87}\text{Rb}$ . The lattice beam is derived from the 1st order diffraction of an acousto-optic modulator (AOM). The lattice is turned ON and OFF by switching the RF power that drives the AOM via a high frequency switch. The pulse ON time for the applied kicks is  $\approx 220$  ns and the free propagation time is kept to be  $\approx 10.6 \mu\text{s}$ . For the parameters used in the experiment, the scaled Planck constant is  $\sim 2$  and the kick strength ( $K$ ) is calculated to be 6 with 10 % uncertainty. For realization of the Lévy noise, a sequence of wait times following Lévy statistics are fed to an arbitrary waveform generator which in turn controls the RF switch of the AOM driver. The presented experimental data for each Lévy exponent is an average over five different noise realizations.

Figure 1(a) shows one realization of the actual kicking sequence used in the experiment for several values of Lévy exponent  $\alpha$ . As  $\alpha$  increases, the mean number of missed kicks decreases such that in the limit of  $\alpha \rightarrow \infty$  it is effectively a periodic kick sequence. In this limit, we expect the system to display the properties of standard kicked rotor system, i.e., Eq. 1 with  $g_n = 0$  for all  $n$ . In Fig. 1(b), the mean energy growth of the system for  $K = 6$ ,  $\hbar_s = 2$  while the Lévy exponent  $\alpha$  is varied. In this, symbols with error bar represent experimental data while dashed lines are the numerical results. It can be immediately recognized that the diffusion shows an unusual property, namely, non-monotonicity as a function of  $\alpha$ . As  $\alpha$  is tuned from 2.0 to 10.0, diffusion reaches a maximum at about  $\alpha \approx 4.0$  and then begins to decrease.

To obtain a broader perspective of this result, for an arbitrarily chosen time  $t = \bar{t}$ , the mean energy  $\langle E \rangle_{\bar{t}}$  is tracked as a function of  $\alpha$ . In Fig 1(b),  $\langle E \rangle_{\bar{t}}$  at a fixed time of  $t = 77$  (in units of kick period) is displayed as a function of  $\alpha$  for the case of kick strength  $K = 6.0$  and  $\hbar_s = 2.0$ . It is apparent that  $D$  has non-monotonic dependence on  $\alpha$  such that its maxima occurs at  $\alpha = \alpha_c$ . The symbols with error bars represent experimental data, and the dashed line is the analytical expression in Eq. (7), in which the break-time,  $t^*$  is treated as a fitting parameter. The best estimate of the break-time  $t^* = 7.27$  (in units of kick period) obtained through fitting is very close to the theoretical prediction  $t^* \sim \frac{K^2}{\hbar_s^2} = 9$ . Clearly, the experimental data displays an excellent agreement with the theoretical result in Eq. (7). Fig. 1(c) displays an unusual feature that  $\langle E \rangle_t$ , at  $t = 77$ , initially increases with  $\alpha$  until  $\alpha < \alpha_c$ , and begins to decay for  $\alpha > \alpha_c$ . In this case, the mean energy growth is maximum at  $\alpha = \alpha_c \approx 4.0$ . The choice of  $t = 77$  is for illustrative purposes and a similar behaviour with identical value of  $\alpha_c$  is obtained for any other  $t$ , provided other parameters are held constant.

This can be understood as follows. Note that the contribution to mean energy due to  $I_2$  is negative and hence acts to suppress the growth of mean energy. On the other hand,  $I_3 > 0$  and tends to increase mean energy. The competition between these two terms leads to a maxima

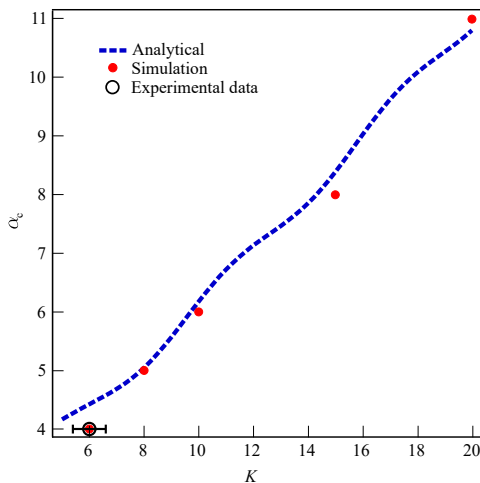


FIG. 3. The variation of critical exponent  $\alpha_c$  as a function of  $\frac{K}{\hbar_s}$ , where  $\hbar_s = 2$  and  $K$  is a free variable. Dashed line is the plot of analytical expression given in Eq.8 and symbols represent the values of  $\alpha_c$  as observed in the numerical simulations. At  $K = 6$ , experimental data for  $\alpha_c$  from Fig. 1(c) is also shown.

at  $\alpha = \alpha_c$ , as seen in Fig. 1(c). Physically,  $I_2$  originates due to the noisy kick sequence and is related to the probability of missing a kick at a given time instant. The exponent  $\alpha$  present in  $I_2$  controls the mean number of missed kicks. As  $\alpha$  increases, fewer kicks are missed, and hence the mean energy increases. The term  $I_3$  arises from decoherence of the localized state and is therefore associated with delocalization and consequent increase of mean energy. Since the signs of  $I_2$  and  $I_3$  are opposites of one another, the net effect of these two competing terms leads to a maxima in mean energy growth at  $\alpha = \alpha_c$ . Presence of a single maxima is due to monotonic behaviour of  $I_2$  and  $I_3$  respectively as a function of  $\alpha$ .

Further, we explore the limit of  $\alpha \rightarrow \infty$ . For any fixed value of  $t$  such that  $t \gg t^*$  and now if the limit  $\alpha \gg \alpha_c$  is taken, both  $I_2$  and  $I_3$  tends to zero. This leads to  $\langle E \rangle \sim K^2/2$ , a time-independent value that corresponding to that of the localized state obtained with periodic kicking. For large  $\alpha$ , the mean number of missed kicks becomes vanishingly small and hence the system essentially works like the standard kicked rotor. As observed in Fig. 1(c), for large  $\alpha$ , the mean energy is seen to be approaching a constant value. This constant value of  $K^2/2 = 18$  is approached very slowly since  $D \propto \alpha^{-1}$  as  $\alpha \rightarrow \infty$ .

In Fig. 2(a,b), numerically simulated energy diffusion of the system in Eq. (1) is displayed for kick strengths  $K = 10$  and  $K = 15$  respectively. It can be noticed from this figure that  $\alpha_c$  depends on the kick strengths. For  $K = 10$ ,  $\alpha_c \approx 6$  and for  $K = 15$ , we obtain  $\alpha_c \approx 8$ . These numerical estimates of  $\alpha_c$  are in accordance with that predicted by the analytical expression in Eq. (8). Hence, the results shown in Fig. 1(b,c) repeats itself qualitatively for other values of kick strengths as well except that  $\alpha_c$  at which the diffusion is maximum

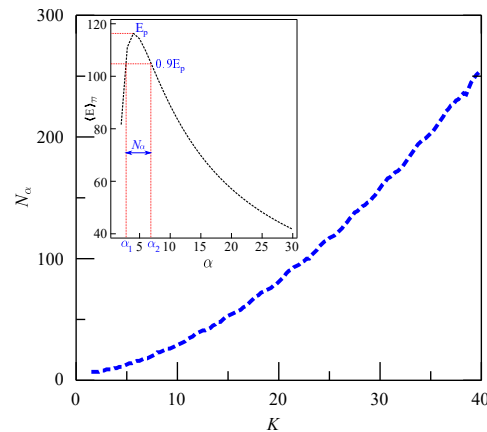


FIG. 4. Variation of  $N_\alpha (= \alpha_2 - \alpha_1)$  with kick strength  $K$ .  $\alpha_1, \alpha_2$  are the values of  $\alpha$  where the energy is 90% of the energy at  $\alpha_c$ . Inset shows a replica of fig. 1(c) with  $E_p$  being the energy at  $\alpha_c$  and  $N_\alpha$  shows the width in  $\alpha$  at energy equals to  $0.9E_p$ .

depends on  $K$ . For a fixed value time  $t = \bar{t}$ , starting from Eq. 7 an expression for  $\alpha_c$  is derived by extremizing  $D$  with respect to  $\alpha$  and it gives,

$$\alpha_c = \frac{1 + \sqrt{(1-q^2)t^*}}{1 - \frac{1}{(1-q^2)t^*}}. \quad (8)$$

In this,  $q \equiv q(K'_n/\hbar_s)$  and  $t^* \equiv t^*(K/\hbar_s)$ . Hence,  $\alpha_c$  depends only on the ratio  $\frac{K}{\hbar_s}$ . Figure 3, shows  $\alpha_c$  as a function of  $K$  for a fixed value of  $\hbar_s$ . In this figure, the result of Eq. 8 is matched against the numerical simulations of quantum Levy kicked rotor. The experimentally obtained data point for  $K = 6$  is also shown. To a first approximation,  $\alpha_c$  increases linearly with  $K$  and the agreement with simulation and experimental result is good. This result also emphasises the quantum nature of the non-monotonic diffusion in Levy kicked rotor. As  $\hbar \rightarrow 0$ , in the semiclassical limit,  $K/\hbar \gg 1$  and hence  $\alpha_c \rightarrow \infty$ . Hence, the non-monotonic diffusion is a quantum phenomenon and cannot be seen in the classical Levy kicked rotor. Indeed, in the classical numerical simulations (not shown here) of this system, the diffusion is indeed monotonic for all values of  $K$ .

Another feature that can be inferred from Fig. 2 is that for large kick strengths such as  $K \gtrsim 10$ , the curves for  $\langle E \rangle_t$  corresponding to different values of  $\alpha$  are tend to be close each other or even overlap. However, for  $K = 6$  in Fig. 1, as  $\alpha$  is varied  $\langle E \rangle_t$  remains quite distinct. The extent to which the system responds to variation in Levy exponent  $\alpha$  can be quantified by a "response" curve defined as follows. We define a "bandwidth" in  $\alpha$  space defined as  $N_\alpha = \alpha_2 - \alpha_1$ , in which  $\alpha_1$  and  $\alpha_2$  are such that

$$\langle E \rangle_t(\alpha_1) = \langle E \rangle_t(\alpha_2) = 0.9\langle E \rangle_t(\alpha_c). \quad (9)$$

Thus, in analogy with  $Q$ -values of oscillators, smaller values of  $N_\alpha$  would correspond to higher sensitivity of the

system to changes in  $\alpha$  in stark contrast to larger  $N_\alpha$  corresponding to lower sensitivity. Figure 4 shows  $N_\alpha$  obtained through numerical simulations starting from Eq. 6. The inset in this figure pictorially illustrates the definition of  $N_\alpha$  for the data shown in Fig. 1(c). It is seen that as  $K$  increases,  $N_\alpha$  increases pointing to increasing loss of sensitivity to changes in  $\alpha$  for large kick strengths. This behaviour of  $N_\alpha$  explains why  $\langle E \rangle_t$  curves nearly overlap for large  $K$ . If  $K \gg 1$ , there is a wide band of  $\alpha$  values for which diffusion rates are nearly same as that at  $\alpha_c$ . Physically, it is reasonable to expect that large kick strengths are classically chaotic regimes, and the kicked rotor is less sensitive to variations in  $\alpha$ .

In summary, the dynamics of Lévy kicked rotor system is studied through experiments and simulations in the regime of Lévy exponent  $\alpha > 1$ . In this, instead of periodic kicking of the standard kicked rotor, the sys-

tem misses kicks at time intervals governed by the Lévy waiting time distribution,  $w(\tau) \sim \tau^{-1-\alpha}$ . For  $\alpha > 1$ , the mean waiting time  $\bar{\tau} = \frac{\alpha}{\alpha-1}$ . The central result is the non-monotonic behavior of diffusion coefficient upon variation of  $\alpha$ . In general, for any value of kick strength  $K$  such that the system is classically chaotic, the diffusion rate as a function of  $\alpha$  displays a single maximum at  $\alpha = \alpha_c$ . It is also shown that  $\alpha_c$  is linearly dependent on  $K/\hbar_s$ , showing that the non-monotonicity of diffusion is a quantum effect that vanishes in the classical limit. Non-monotonicity of diffusion is a surprising feature that is generally not seen in the standard quantum kicked rotor and its variants.

Sanku Paul and Sumit Sarkar contributed equally to this work. Sanku Paul performed theoretical and computational work. Sumit Sarkar was part of the experimental team.

- 
- [1] H. J. Stöckmann, *Quantum Chaos: An Introduction*, Cambridge U.P. (2000).
- [2] F. Haake, *Quantum signatures of chaos* (Springer Science & Business Media, Berlin Heidelberg 2013).
- [3] C. Hainaut, A. Rancon, J-F. Clement et. al., Phys. Rev. A **97**, 061601(R) (2018).
- [4] S. Longhi, Phys. Rev. A **95**, 012125 (2017).
- [5] G. G. Carlo, L. Ermann, A. M. F. Rivas, and M. E. Spina, Phys. Rev. E **93**, 042133 (2016).
- [6] S. Sarkar, S. Paul, C. Vishwakarma, S. Kumar, G. Verma, M. Sainath, Umakant D. Rapol, and M.S. Santhanam, Phys. Rev. Lett. **118**, 174101 (2017).
- [7] D. U. Matrasulov, G. M. Milibaeva, U. R. Salomov, and Bala Sundaram Phys. Rev. E **72**, 016213 (2005).
- [8] Q. Zhao, Cord A. Muller and J. Gong, Phys. Rev. E **90**, 022921 (2014).
- [9] S. Paul, H. Pal and M. S. Santhanam, Phys. Rev. E **93**, 060203(R) (2016). S. Paul and M. S. Santhanam, Phys. Rev. E **97**, 032217 (2018).
- [10] I. Manai, J. F. Clement, R. Chicireanu, C. Hainaut, J. C. Garreau, P. Szriftgiser, and D. Delande, Phys. Rev. Lett. **115**, 240603 (2015).
- [11] F. Revuelta, R. Chacón, and F. Borondo, Phys. Rev. E **98**, 062202 (2018).
- [12] S. Notarnicola, F. Iemini, D. Rossini, R. Fazio, A. Silva, and A. Russomanno, Phys. Rev. E **97**, 022202 (2018).
- [13] P. Qin, A. Andreanov, H. C. Park and S. Flach, Scientific Reports **7**, 41139 (2017)
- [14] L. Huang, Hong-Ya Xu, C. Grebogi, and Y.-C. Lai, Phys. Rep. **753**, 1 (2018). E. B. Rozenbaum and V. Galitski, Phys. Rev. B. **95**, 064303 (2017).
- [15] D. R. Grempel, R. E. Prange, and S. Fishman, Phys. Rev. A **29**, 1639 (1984).
- [16] P. W. Anderson, Phys. Rev. **109**, 1492 (1958); 50 Years of Anderson Localization, edited by E. Abrahams (World Scientific, Singapore, 2010).
- [17] A. Iomin, S. Fishman, and G. M. Zaslavsky, Phys. Rev. E **65**, 036215 (2002).
- [18] M. B. d’Arcy, R. M. Godun, D. Cassettari, and G. S. Summy, Phys. Rev. A **67**, 023605 (2003).
- [19] B. G. Klappauf, W. H. Oskay, D. A. Steck, and M. G. Raizen, Phys. Rev. Lett. **81**, 1203 (1998); D. A. Steck, V. Milner, W. H. Oskay, and M. G. Raizen, Phys. Rev. E **62**, 3461 (2000).
- [20] D. A. Steck, V. Milner, W. H. Oskay, and M. G. Raizen, Phys. Rev. E **62**, 3461 (2000).
- [21] W. H. Oskay, D. A. Steck and M. G. Raizen, Chaos, Solitons & Fractals, **16**, 409 (2003).
- [22] G. M. Zaslavsky, Phys. Rep. **371**, 461 (2002).
- [23] H. Schomerus and E. Lutz, Phys. Rev. A **77**, 062113 (2008).
- [24] H. Schomerus and E. Lutz, Phys. Rev. Lett. **98**, 260401 (2007).
- [25] D. Cohen, Phys. Rev. Lett. **67**, 1945 (1991); D. Cohen, Phys. Rev. A **44**, 2292 (1991).
- [26] J. Schrieffer, M. Clusel, D. Carpentier, and P. Degiovanni, Europhys. Lett. **69**, 156 (2005).